Control of Particle Cohesion with a Polymer Coating and Temperature Adjustment

J. Bouffard, F. Bertrand, and J. Chaouki
Dept. of Chemical Engineering, École Polytechnique de Montréal, P.O. Box 6079, Stn. Centre-Ville, Qc, Canada H3C 3A7

S. Giasson
Dept. of Chemistry and Faculty of Pharmacy, Université de Montréal, C.P. 6128, Stn. Centre-Ville, Montréal, Québec, Canada H3C 3J7

DOI 10.1002/aic.13765
Published online March 29, 2012 in Wiley Online Library (wileyonlinelibrary.com).

A new approach is presented that introduces interparticle forces induced by a change of temperature at which polymer coated particles are exposed. The particle cohesive flow behavior is shown for two different applications. The first one considers a dense granular flow that is typically observed for wet powder granulation using a modified spheronizer. The other application shows the possibility of mimicking the particle flow behavior observed in high-temperature fluidized beds with the advantage of being operated at ambient conditions. For the first application, as the temperature increases, significant changes in the particle bed surface morphology were observed and an important reduction of the dynamic density was noticed. For the gas–solid fluidized-bed application, pressure drop measurements revealed that the behavior of the particles transited from Geldart group B to Geldart group A and even Geldart group C as the temperature increased.
 AIChE J, 58: 3685–3696, 2012
Keywords: particle cohesion, temperature control, dense granular flow, spheronizer, fluidized bed, pressure drop

Introduction

Granular flow dynamics has been already studied with noncohesive and cohesive particles induced by different force types in dense granular systems, as encountered in blenders[1–3] or fluidized-bed applications.[4–7] The presence of cohesive particulate material can induce a change in the flow pattern observed in process equipment when compared to a free-flowing material.[8] It can also lead to the appearance or modification of segregation patterns that are different from the ones in noncohesive cases.[9–11] In order to study and characterize the interparticle force effects on granular flow dynamics, different approaches have been used to introduce cohesive forces into the particulate material.The interparticle force can be chosen to reproduce the conditions found in a real process (e.g., the use of capillary force to study its impact on a wet granulation process), but also to mimick, in a more friendly environment, the cohesive behavior present in a granular application difficult to characterize with experimental measurements because of extreme operating conditions. Fluid beds that operate at high temperature are an example of one such application for which the characterization is limited to optical observations of the process.[12]

The van der Waals forces have a significant impact on the interactions between particles. The cohesive forces that bind two particles are directly proportional to the particle size according to the following equation[13–14]

$$F_{VdW} = \frac{A_H a}{12h^2} \tag{1}$$

where A_H is the Hamaker constant, a is the spherical particle radius, and h is the separation distance between the two particle surfaces, which corresponds to the nearest distance for particles in close contact. When the particles become larger than 100 μm,[15] the van der Waals forces become less significant because of the predominance of the inertial and gravity forces. This leads to a higher mobility of the particles, which is characteristic of the free-flowing behavior.[1] The use of van der Waals forces to study the cohesive behavior is then difficult when large flowing particles are considered. For these particles, the cohesion must be induced by adding a cohesive agent that creates the interparticle forces. One of the most popular methods to induce a cohesive effect inside a particulate material is to introduce wet capillary bonds coming from an interstitial liquid between the particles, as shown in Figure 1.

The capillary force depends on the surface tension and the pressure differential Δ_P across the air-liquid interface, according to the following expression[17]

$$F_{cap} = 2\pi\gamma a \sin\phi \sin(\phi + \theta) + \pi a^2 \Delta p \sin^2\phi \tag{2}$$

where ϕ is the polar position of the liquid bridge edge relative to the particle center and the horizontal reference axis, θ is the

Correspondence concerning this article should be addressed to F. Bertrand at francois.bertrand@polytl.ca or J. Chaouki at jamal.chaouki@polytl.ca.

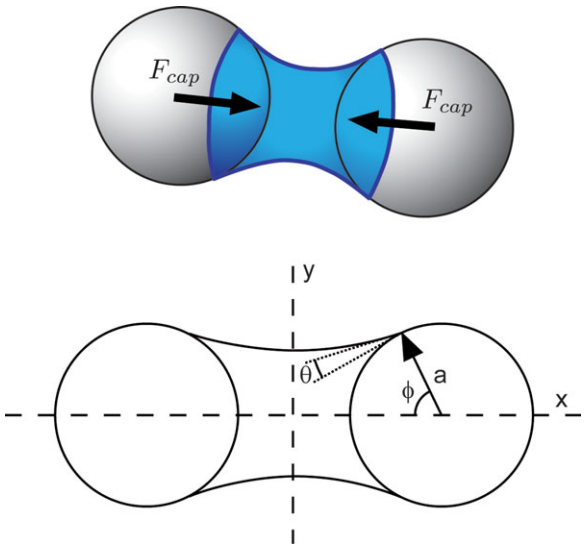

Figure 1. Capillary forces induced by moisture content.[16]

[Color figure can be viewed in the online issue, which is available at wileyonlinelibrary.com.]

contact angle, and a is the particle radius, as defined in Figure 1, and γ is the surface tension. The Laplace pressure depends on the volume of liquid between the particles, which is expressed via the interface profile of the liquid bridge Y

$$\frac{\Delta pa}{\gamma} = \frac{\ddot{Y}}{(1+\dot{Y}^2)^{3/2}} - \frac{1}{Y(1+\dot{Y}^2)^{1/2}} \tag{3}$$

As the moisture content increases, different saturation states are reached, which induce significant changes in the interparticle force.[18] The pendular state is characterized by the presence of capillary bonds linking only two particles at a time, and by the fact that the cohesion is proportional to the quantity of moisture content.[19] The pendular state exists within a low-moisture concentration range (1–3 vol %) for which the control of the liquid distribution throughout the particulate bed can be difficult,[18] and, thus, result in nonhomogeneous interparticle forces throughout the particulate bed.[20]

An alternative way to induce cohesive forces between the particles is by increasing magnetic interactions using the presence of a ferromagnetic component. With this approach, a magnetic field is generated to polarize the particulate material in a specific direction. The poles created inside the particles interact with each other and then induce a cohesive/repulsive behavior. One advantage of using this type of cohesion is the absence of a liquid phase that must be uniformly distributed. Also, since the magnetic force varies with the square of the magnetic field intensity for a constant particle material and size distribution,[21–22] it is relatively easy to introduce and control cohesive interactions within the granular material. The flow behavior of such cohesive material is different from the flow dynamics generally encountered in industrial applications since the cohesive forces are aligned with the magnetic field following a specific direction. Because of the polar interactions, as seen in Figure 2, the cohesive forces are not distributed uniformly around the particles, which induces anisotropic attraction/repulsion forces into the bulk material.[23] Some work has been done to reduce the presence of the force anisotropies by employing a rotating magnetic field,[22] but it does not solve the problem completely since the poles rotate around the particles by following the magnetic field. The magnetic force between two ferromagnetic particles is given in [23]

$$F_{mag} = 12\pi\mu_0\mu_f a^2\vec{B}^2\left(\frac{\mu_p - 1}{\mu_p + 2}\right)^2 \vec{f}(r,\alpha) \tag{4}$$

where μ_0 is the magnetic constant, μ_f and μ_p are the fluid and particle relative magnetic permeabilities, respectively, $\vec{B}$ is the magnetic field, r and α are the distance and the angle between the two particles, respectively, $\vec{f}$ is the secondary field created by the magnetization of one particle, and a is the particle radius. Note that this secondary field due to neighboring material affects the cohesive force induced by the principal magnetic field on a specific particle.

It has been shown that the aforementioned approaches have inherent limitations with respect to the control of interparticle forces, independent of the particle size, and/or the cohesive force uniformity throughout the particulate bed, which come from inherent physical limitations (distribution or evaporation of a liquid or magnetic force anisotropy). Modification of the particle surface properties is another way to induce cohesive effects throughout the particle bed. Different approaches can be used to modify the cohesive forces, such as a change of roughness[24] or the addition of nanoparticles by dry coating.[25–26] In such cases, a reduction of the cohesion is normally desired and cohesion adjustment is not necessarily the objective. The control of surface cohesion can also be achieved by coating the surface with a polymer. This approach, relatively well understood in the case of binary surface contacts, allow adhesion and friction to be controlled.[27–30]

In this article, we propose to use a polymer coating and temperature adjustment to control interparticle forces within a granular material and ensure their homogeneous distribution throughout the particulate bed. To do so, we have applied this new technique to two different cases: in a spheronizer, which is characterized by a dense particle flow regime, and in a fluidized bed where the flow is fluid-like or gaseous. Description of the mechanisms involved during the polymer adhesion are first explained. The interparticle forces between coated particles with respect to their size and the

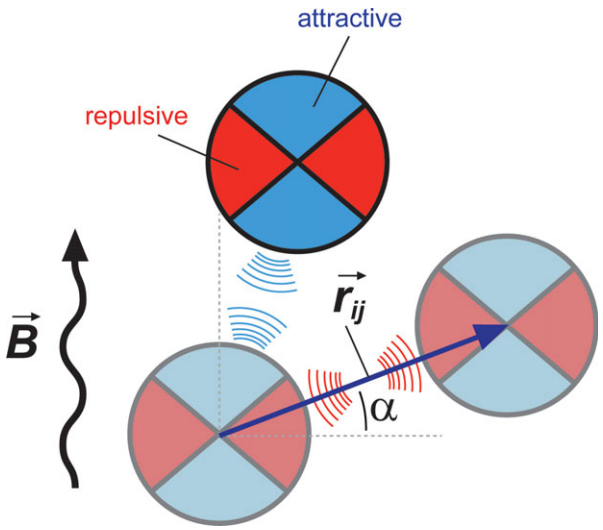

Figure 2. Magnetic field interaction with ferromagnetic particles (modified from ref. 23).

[Color figure can be viewed in the online issue, which is available at wileyonlinelibrary.com.]

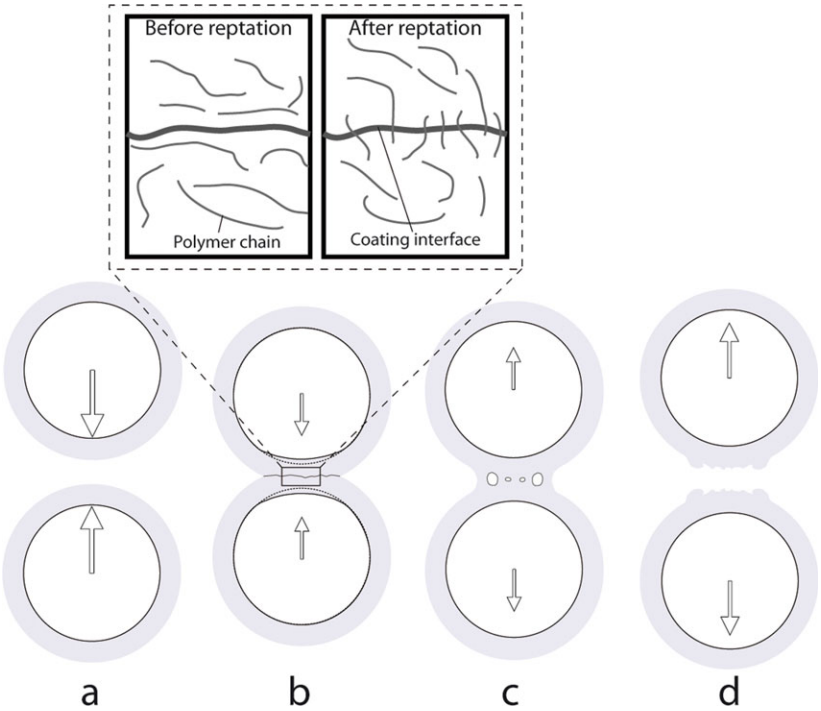

Figure 3. Collision of two coated particles (a) particles before collision, (b) molecular interdiffusion of the polymer layers occurring during contact and deformation. The polymer chain ends cross the interface following a reptation mechanism, (c) separation of the particles with cavity formation. Entanglement of the polymer chains induces adhesive forces when the particles are separated, and (d) formation of craters following the complete separation of the particles.

[Color figure can be viewed in the online issue, which is available at wileyonlinelibrary.com.]

process temperature were measured using a surface forces apparatus (SFA). Common interparticle forces generally encountered in particle applications are compared to the estimated polymer forces. The cohesive flow behavior in the spheronizer with the coated particles is qualitatively and quantitatively assessed for different temperatures through bed-surface vizualization and particle-bed density measurements. Finally, the behavior of coated particles in a fluidized bed is characterized through pressure drop and bed-height measurements, and the results are compared with data from the literature obtained with other particle systems.

Polymer coating approach

The adhesion force between two polymer layers in contact strongly depends on the interdiffusion rate of the polymer chains, the area of contact, the contacting time, the compression between the layers and the decompression rate. Above the glass transition temperature, the polymer chains are able to move following a process of reptation and they can cross the interface created.[31] Figure 3 presents the cohesion mechanism when two coated particles collide at a temperature that is over the glass transition state. Upon colliding, the two polymer layers are deformed and create a ''meniscus'' across the interface. During this step, a molecular interdiffusion of the polymer chains takes place. The interdiffusion rate between these chains depends mainly on the polymer chain molecular weight, the level of entanglement and the process temperature.[32–33] As the molecular chains diffuse, the polymer relaxes and the interface disappears for a contact duration that equals the reptation time (τ_D), which depends on the diffusion of these polymer chains[33–34]

$$\tau_D = \frac{2R_g^2}{\pi^2 D_{\text{Rept}}} \tag{5}$$

where R_g is the radius of gyration of the polymer chain, D_{Rept} is the reptation diffusion coefficient. The reptation time at temperature T can be estimated by the William-Landel-Ferry empirical model

$$\log\left(\frac{\tau_D}{\tau_R}\right) = \frac{-c_1(T - T_R)}{c_2 + (T - T_R)} \tag{6}$$

where τ_R is the reference reptation time at temperature T_R, and C_1 and C_2 are regression constants that depend on the polymer species. The reptation time then depends on the polymer properties and decreases significantly above the glass transition state. For example, for PEA with a molecular chain weight in the order of 10^5 kg/mol, the reptation time is around 5 h when the temperature is 270 K, while it is around 10 s for a temperature of 340 K.[35] As the polymer chains diffuse through the interface, the resultant adhesion force increases. The adhesion energy per unit area necessary to separate two layers of polymer completely is defined by[36]

$$W_{Adh} = h_0 \int_0^{\varepsilon_{\max}} \sigma d\varepsilon \tag{7}$$

where h_0 is the initial polymer layer thickness, and ς and $\varepsilon_{\max}$ are the stress and maximum strain, respectively. The stress depends on the strain but also on the debonding rate and the polymer chain weight. The adhesion energy can also be estimated from force/distance curves on approaching and separating of

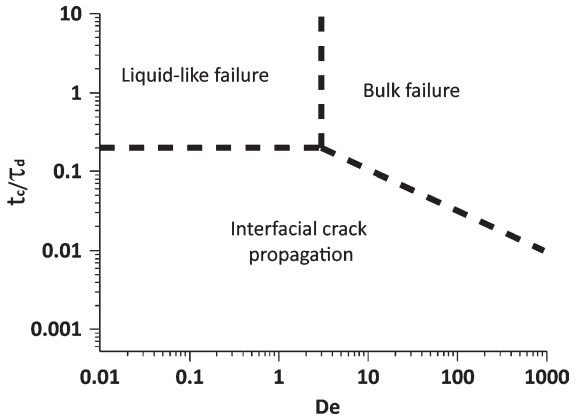

Figure 4. Failure mechanism map as a function of the normalized contact time and the Deborah number.[36]

contacting elastic materials using the JKR theory.[37] In practice, the adhesion energy and the elastic modulus of the material are usually obtained through the JKR equation by measuring and plotting the contact area against the applied load. When the surfaces or particles are pulled apart by a constant force F, they will detach from each other when reaches the adhesion force, which is also called pull-off force (F_P)given by

$$W_{Adh} = \frac{2F_P(R_i + R_j)}{3\pi R_i R_j} \tag{8}$$

where R is the radius of particles i or j.[38–40] This equation can be used in conjunction with SFA measurements of the pull-off force to estimate the adhesion energy.

When two polymer layers are separated with a high-debonding velocity (V_d), the adhesion energy increases with the contact time (t_c), until it reaches a maximum value W_m, which happens in the vicinity of the reptation time (τ_D).[41–42] When the polymer layers are separated slowly or when the contact time is larger than the reptation time, the adhesion energy can be considered constant at the maximum value W_m. Dimensional analysis can be used to describe the failure regime in which the contacting polymer layers are debonded. The first dimensionless number is the ratio between the contact time and the reptation time (T_d/τ_D), named the normalized contact time. The second is the Deborah number, which is defined by

$$De = \frac{V_d \tau_D}{h_0} \tag{9}$$

where V_d/h_0 is the average initial strain rate. The Deborah number represents the ratio between the material relaxation time following a deformation and the characteristic time scale of the process. Figure 4 shows the three different failure mechanisms encountered, depending on these two dimensionless numbers. The liquid-like and the bulk failure mechanisms occur when T_d/τ_D is large and are then associated with the maximum value of the adhesion energy W_m, while the presence of interfacial cracks indicates that the adhesion energy is not at equilibrium and increases with the contact time.[36,41] The liquid-like failure is observed when the debonding rate is low enough (low De) and T_d/τ_D has no effect on the adhesive energy. This separation regime should not be expected in spheronizer or fluidized-bed applications. At high-debonding rate (high De), if the bulk failure is observed, it means that the polymer layers are strongly deformed. Because it may result in a layer breakage, this separation regime is not desired and must be avoided to ensure the coated particle integrity.

The particle contact time (t_c) between particles is not easy to evaluate for a dense particle flow regime. The Hookean relation used for elastic particles can give an estimate of t_c in such a situation, but it requires simulations of particulate flow to set key parameters such as the stiffness and the damping coefficients on the basis of experimental results.[43] Timoshenko and Goodier[44] developed an empirical relation that can approximate the contact time for elastic spheres

$$t_c = 2.94\left(\frac{5\sqrt{2}\pi\rho}{4}\frac{1-\upsilon^2}{E}\right)^{2/5}\frac{a}{v_n^{1/5}} \tag{10}$$

where ρ is the particle density, υ is the Poisson ratio, E is the Young's modulus, a is the particle radius and v_n is the normal collision velocity, which is estimated by the product of the particle size and the shear rate ($v_n = a\dot{\gamma}$).[45] Due to the absence of a viscous relaxation term, the contact time calculated by this relation represents a low-limit value. Nevertheless, it can be used to estimate an effective adhesion energy from[46]

$$W = W_m\left\lfloor 1 - \exp\left(-at_c^b\right)\right\rfloor \tag{11}$$

where the regression constants a and b vary with the polymer properties such as the molecular weight, the reptation time and the polymer structure.

As previously mentioned, the measured adhesion force strongly depends on the contact area and the contacting time between the polymer layers. Therefore, it is dependent on the viscoelastic behavior of the polymer. When the polymer is in the rubbery regime over its glass transition value, the elastic modulus decreases with an increase in temperature, which allows the polymer layer to deform more easily. The thickness of the layer has an impact on the maximum deformation that can be reached and the resulting contact area created. In fact, it has been shown that a decrease in coating thickness reduces the adhesion between the contacting layers.[42]

Methodology

The experimental work first required the production of particles from fine pharmaceutical excipients. These particles were then coated with a polymer film using an atomization process to obtain a uniform coating layer on their surface. After these preparation steps, the particulate material was used inside a spheronizer equipment and submitted to different temperatures that altered the polymer properties and the cohesive forces.

Particle production process

Table 1 shows the process equipment used to produce the particles for the experimental work. A preliminary mixing step with a high-shear mixer served to blend the powder materials (Table 2). When the powder was homogeneously mixed, a binder solution (Table 2) was added to the high-shear mixer to granulate and color the material. The newly formed granules were then fed to an extruder and the resulting product was transferred to a spheronizer to create spherical beads. These beads were dried in a tray dryer. After the production process, the particles were spherical, as evidenced in the SEM picture of Figure 5, and characterized by a

Table 1. Process Parameters for the Equipment used for the Production of Particles

Equipment	Parameters
High shear mixer Fukae Powtec LFD-GS2J	Main agitator: 300 rpm Secondary agitator: 1000 rpm Solution flow rate: 60 g/min
Extruder LCI Multi Granulator MG-55	Screw rotational rate: 30 rpm Mesh size: 1.2 mm
Spheronizer LCI Marumerizer Model QJ-230T	Disk rotational rate: 1000 rpm Spheronization time: 10 min
Tray dryer	Temperature: 60°C Drying time: 2 h

narrow particle size distribution with a mean size of 1.2 mm (Figure 6).

Particle coating process

The next step consisted of adding a polymer layer onto the surface of the particles. To achieve this task, a spheronizer (Caleva 380), different from the one used for the particle production process, was modified to incorporate an air line located below the rotating disc. The introduction of air helps to prevent infiltration of particulate material from the bed through the spheronizer gap located between the rotating disc and the wall. Before entering the spheronizer bowl, the air passes through an electrical heater to adjust its temperature to the desired process setpoint. The temperature is set using a controller coupled with a thermocouple that measures the temperature at the entrance. To ensure that the temperature of the particles reaches steady state, an infrared cell is located at the top of the spheronizer to measure the temperature at the surface of the particulate material. The airflow rate is adjusted with a valve at the entrance of the equipment to the desired value with the help of a gas rotameter. Table 3 presents the parameters associated with the coating process (Figure 7). During the experiment, the disc rotational speed was set to provide adequate particle mixing but also to prevent the breakage of the particles due to a large-shear rate. The airflow rate and the temperature were adjusted to ensure a sufficient drying rate during the coating process and to avoid particle adhesion, respectively. The particles were coated with the polymer suspension, whose composition is indicated in Table 4. It consists of a solution of a PEA/PMMA copolymer in a 2 to 1 ratio, which induces the cohesive effect, and nonoxynol, a surfactant employed to synthesize the polymer by emulsion polymerization. Two different quantities of this polymer suspension (commercial name Eudragit® NE30D) were added to the batches in the proportions indicated in Table 5. The coating layer thicknesses indicated in this table were estimated by assuming an equal distribution of the polymer dry mass on all the particles while taking into account the particle-size distribution presented in Figure 6. The coating suspension

Table 2. Powder and Solution used for the Production of the Particles

Elements	Materials	Quantity (kg)
Powder blend	MCC PH-101	0.200
	Lactose monohydrate	0.200
	NaCl	0.100
Binder solution	Water	0.315
	NaCl	0.095
	Yellow quinoline	0.002

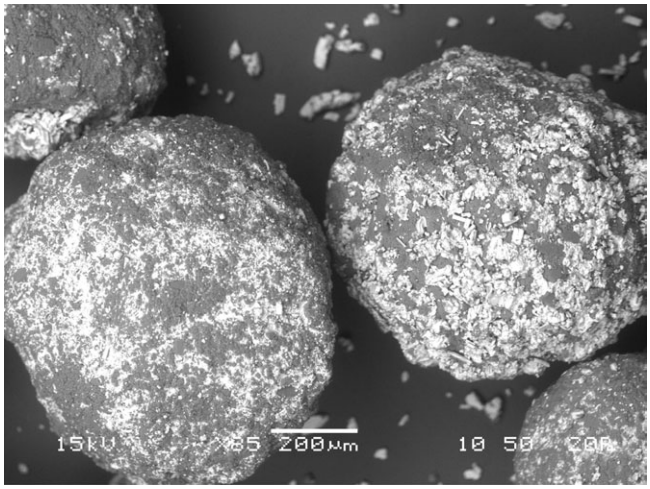

Figure 5. SEM picture of the uncoated spherical beads.

was coated onto the particles by atomization with a two-fluid atomizer (BETE XA-SR 050). It was fed by a peristaltic pump at a flow rate equal to approximatively 1 g/min using compressed air to allow for the formation of fine droplets. The atomizer was positioned so that the tip of the nozzle was at a distance of 4 cm from the bed surface to avoid coating losses to the mechanical parts of the spheronizer. Figure 8 shows the appearance of the coated particles at the end of the coating process.

Measurement of the surface morphology and dynamic density

The surface of the torus of particles inside the spheronizer (Caleva 380) was characterized by pictures taken with a digital camera. The change of surface morphology was linked to the modification of cohesion forces as the temperature increased. The pictures were acquired under the process conditions presented in Table 6. These parameters were kept constant for all the tests, except for the temperature of the particulate bed, which was increased by 1°C increments during each experiment. The range of temperatures selected was above the glass transition temperature of the polymer, and was set to obtain a variation of the cohesive behavior. The airflow rate was set to a low value to modify the temperature of the particles and to avoid infiltration of material below the processing chamber of the spheronizer. Between 12 to 15 cfm, the airflow rate induced no significant changes on

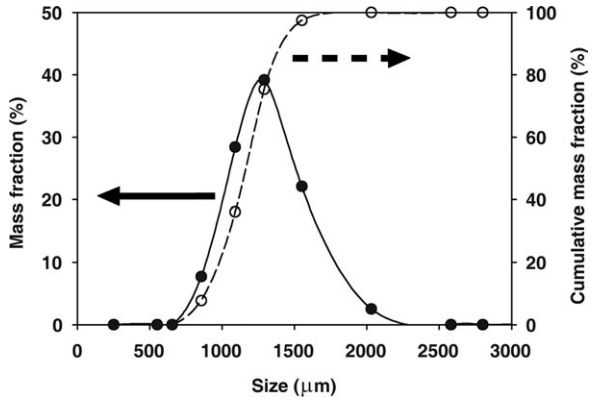

Figure 6. Particle-size distribution of the particles used in this work.

Table 3. Coating Process Parameters

Parameters	Values
Disc rotational rate	230 rpm
Air flow rate	42.5 m^3/h
Air temperature	30°C
Solution flow rate	1 g/min
Atomization pressure	200 kPa

the particulate flow behavior when compared to the process operated with the absence of incoming air. Figure 9 shows the equipment used to measure accurately the surface position while the spheronizer was in operation. A 2800 LLT Scancontrol laser sheet profiler (microepsilon) measured the mean surface position that was used to calculate the volume of the torus. The dynamic density was obtained by dividing the total particle mass by the calculated volume.

Measurement of the polymer film properties

The glass transition temperature (T_g) was measured with a DSC Q1000 (TA Instruments, USA). The samples of the free polymer film were processed under nitrogen atmosphere at heating and cooling rates of 10°C/min between 20 and 170°C. The glass transition temperature obtained was around −6°C. The pull-off force between two curved mica surfaces (geometry of a sphere of 2 cm radius on a flat surface) coated with the polymer was measured using a surface forces apparatus (SFA) for different temperatures. Spin coating was used for coating the mica surfaces with the polymer. Briefly, a basic SFA allows the normal interaction forces between two surfaces to be determined as a function of the surface separation distance by measuring the deflection of a spring that supports the lower surface as this separation distance is changed. The distance between the two surfaces is determined with a resolution of about 0.2 nm using the standard interferometry technique that uses fringes of equal chromatic order. More details related to this measurement technique can be found in Heuberger et al.[47] For each measurement, the compression load was constant (1 mN), the contacting time was 1 min, and the decompression rate was kept constant (12.5 nm/s). Temperature within the SFA chamber was controlled within 1°C.

Gas–solid fluidized-bed study and analysis method

This part of the experimental work involved a 400–800 μm distribution of spherical sugar beads (dp = 600.5 μm, ρ_p = 1,563 kg/m^3), which belong to the Geldart Group B. These sugar beads were coated with the same PEA/PMMA suspension and procedure as in the case of the spheronizer. The characteristics of the final product are summarized in Table 7.

The experimental setup consists of a fluidization column, which was constructed with a transparent Plexiglas tube, 0.152 m I.D. and 1.5 m in height. Dried and filtered air was distributed into the bed using a perforated plate. It contains holes of 1 mm in diameter and arranged in a triangular pitch.

Air was heated with the help of an electrical heater before entering the fluidization column. It was used to adjust the temperature of the bed to the desired value. Temperature was controlled by means of a PI controller driven by a thermocouple immersed in the bed. A thermocouple located at the windbox allowed measuring the air entrance temperature. The airflow rate was controlled with a rotameter, which confirmed a maximum superficial gas velocity of 0.75 m/s in the bed. Note that different superficial gas velocities were used for covering both the fixed-bed state and the bubbling regime.

To investigate the effect of the cohesive forces on the fluidization behavior, two systems were studied, one with uncoated sugar beads and another with coated sugar beads. Experiments with uncoated sugar beads were carried out at 20°C, while the ones with coated sugar beads were conducted at 20, 30, and 40°C. Hereafter, for simplicity, we name these systems after their different operating conditions in abbreviated form: SB, CSB20, CSB30 and CSB40, which stand for uncoated sugar beads at 20°C, and coated sugar beads at 20, 30, and 40°C, respectively. All experiments were performed at atmospheric pressure. It is worth noting that measured variations in the air density and viscosity in the 20–40°C temperature range were 6 and 5%, respectively, which are fairly negligible compared to the cohesion differences obtained with the proposed technique for the same temperature range. Moreover, the same amount of material was poured into the bed in all cases, which resulted in an initial bed height of approximately 20 cm at ambient conditions. For each temperature considered, the height of the bed

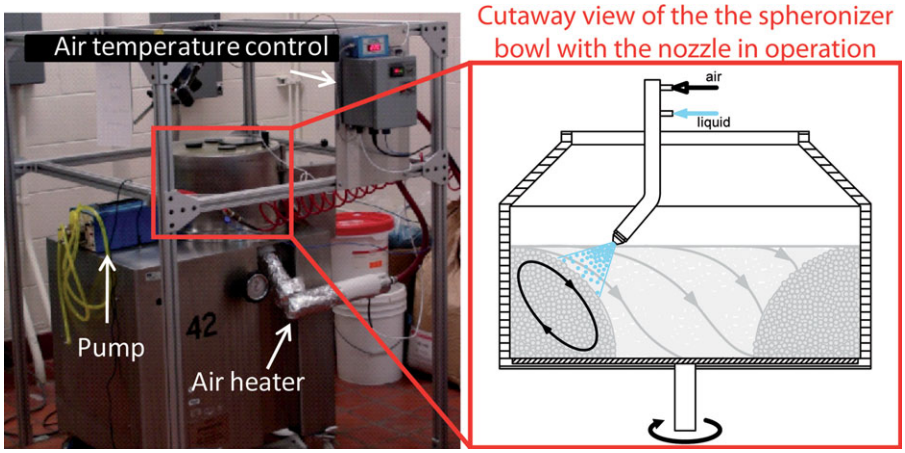

Figure 7. Process used to coat the particles with the polymer.

An atomizing nozzle has been inserted at the top of the spheronizer bowl to spray the coating solution at the surface of the particle bed. [Color figure can be viewed in the online issue, which is available at wileyonlinelibrary.com.]

Table 4. Coating Suspension of Eudragit® NE30D

Materials	Mass %
Water	68.5
PEA/PMMA 2:1	30.0
Nonoxynol 100	1.5

was measured while the airflow rate was slowly decreased to zero, causing the particle flow behavior to change from the fluidized-bed state toward the fixed-bed state.

The pressure drop across the bed was measured using a differential pressure transducer. It was mounted flush with the wall of the column through 15-micron inline filters and measuring ports. In particular, the ratio between the measured and calculated pressure drops across the bed $\Delta P_m/\Delta P_c$, was used to highlight changes in the fluidization behavior of the coated sugar beads with increasing temperature. Note that ΔP_c was calculated by dividing the bed weight by the cross-sectional area of the fluidized-bed column.

Results and Discussion

In the first place, a relationship between the interparticle forces and the macroscopic flow observed in both the spheronizer and the fluidized bed is established with the help of the SFA measurements. The effects of the temperature and the coating thickness on the interparticle forces for the spheronizer application are then discussed on the basis of surface morphology measurements. The flowability of the particles with respect to the temperature is next analyzed using observed variations of the dynamic density measured with the laser sheet profiler. The last part of this section deals with the fluidized-bed application and focuses on a comparison between the results obtained in this work and those reported elsewhere[48] in the case of other types of cohesive particles in fluidization columns operated at high temperature.

Relation between the cohesive forces and the macroscopic flow of the particles in the spheronizer

Equation 8 can be used to estimate adhesion energy W_{Adh} from the pull-off force measured between two curved mica surfaces covered with a 120 nm-thick polymer layer film. As can be seen in Figure 10a, the pull-off force and, as a result, the adhesion energy vary linearly with the temperature. Of course, the polymer thickness also has an impact and must be taken into account. The particles used in this work have a polymer coating thickness varying between 3.5 to 7 μm. Luengo et al.[42] observed that increasing the coating thickness by 1,000 times, from around 2 nm to typically 2 μm, results in an increment in the adhesion energy by approximately the same factor. They suggested that the adhesion energy is proportionnal to the coating thickness. Recent SFA measurements on our system (Eudragit polymer) have also indicated a considerable increase in the pull-off force when increasing the polymer thickness (not shown here). Based on this observation, an effective adhesion energy was evaluated for our particles using Eq. 11, where W_m is the adhesion energy that we measured with the SFA and adjusted with respect to the coating thickness. Note that the high level of adhesion energy obtained is explained by the long contact time (1 min) considered for the SFA measurements. The contact time was estimated from Eq. 10 using a shear rate of $\dot{\gamma} = 1\ s^{-1}$. Because the constants a and b are not known for Eudragit, we used reported values for polyisobutylene (a = 0.9 and b = 0.4) with a comparable maximum adhesive energy and molecular chain weight (10^5 g/mol).[46]

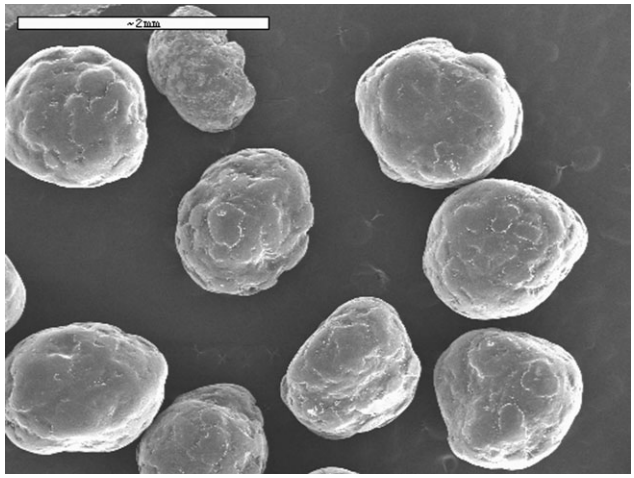

Figure 8. SEM picture of the Eudragit® coated particles.

The interparticle forces, for thin (3.5 μm) and thick (7 μm) polymer coatings and different temperatures were calculated from the corresponding effective adhesion energy values using Eq. 8, are compared to other common forces. It reveals that large variations of interparticle forces can be obtained with the polymer coating approach. It can be noticed that the forces resulting from the thin and thick polymer coatings overlap both the capillary and the van der Waals force ranges. For the thick polymer coating at 45°C, the polymer-induced adhesion force overcomes the other forces. As discussed later, the presence of these strong forces create cohesive phenomena that have not been observed with the other approaches used to generate particle cohesion in granular systems.

Torus surface morphology with respect to temperature

Figures 11 and 12 show the particles in the spheronizer when they are submitted to different operating temperatures. When the spheronizer was operated near the laboratory conditions (20°C), the particles were able to flow freely throughout the torus. The surface is characterized by a smooth profile that subsists until the temperature reaches 44°C (respectively, 40°C) for the thin (resp. thick) coatings. As the temperature was increased to 45°C (respectively,

Table 5. Final Particle Coating Characteristics

Materials	Thin	Thick
Spherical particles (kg)	3	3
Eudragit® coating (kg)	0.045	0.090
Percentage of coating (%wt)	1.5	3.0
Coating layer thickness (μm)	≈ 3.5	≈ 7

Table 6. Operating Parameters for the Spheronizer

Parameters	Values
Disc rotational rate	230 rpm
Air flow rate	20.4-25.5 m^3/h
Temperature range	20-50°C
Particle bed mass	3 kg

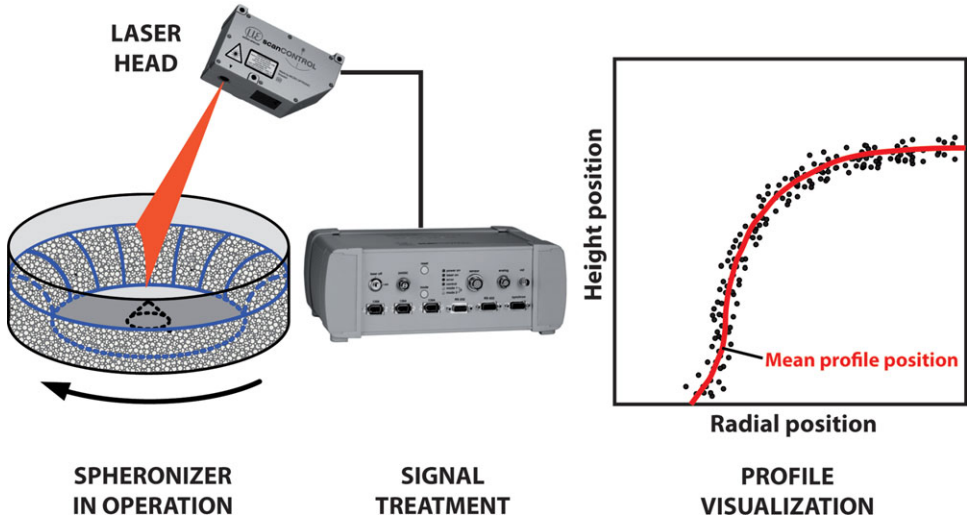

Figure 9. Surface measurement setup with the laser sheet profiler.

The laser head projects a laser line on the particle bed and the light reflected is recorded by a CCD camera located in the same device. The signal is then transfered to the controller box, which evaluates the profile position, in two dimensions, using the triangulation principle. [Color figure can be viewed in the online issue, which is available at wileyonlinelibrary.com.]

41°C), the particles remained in a free-flowing state yet they began to create weak clusters that produced a bumpy torus surface. These clusters became sturdier and larger when the temperature reached 46°C (respectively, 42°C). For the thinly coated particles, the growth and consolidation of these agglomerates continued until the maximum temperature investigated, 48°C, was attained.

For the thickly coated particles, a sudden modification of the torus shape occurred when the temperature approached 43°C. At this point, the appearance of a secondary flow layer on top of the first one and near the spheronizer wall revealed a modification of the particle flow pattern. A small fraction of the material located in this new layer was then observed to continuously disaggregate creating agglomerates at the surface of the underneath free-flowing layer. Some material located in either of the two layers remained unsegregated as it was able to move from one zone to the other by the

Table 7. Final Particle Coating Characteristics for the Fluidized-Bed Experiments

Materials	Quantity
Spherical sugar beads	3.0 (kg)
PMMA/PEA	0.10 (kg)
Mass percentage of coating	3.4 %
Coating layer thickness	$\sim 5\mu$m

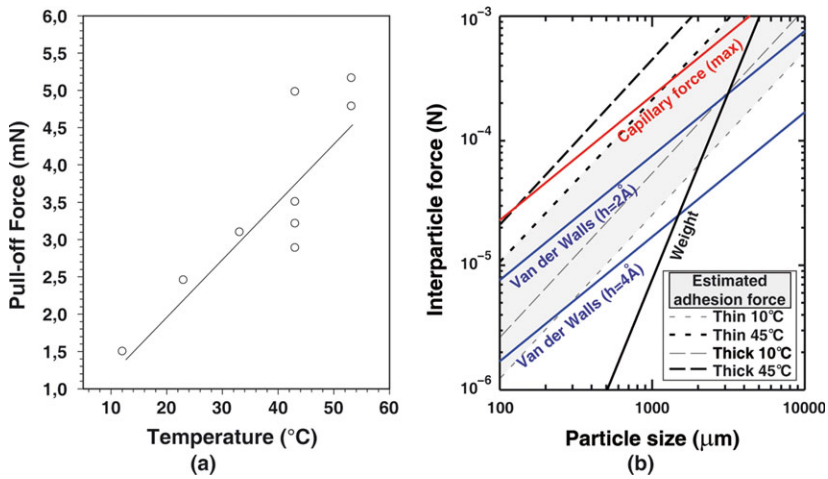

Figure 10. Variation of the interparticle force as a function of the temperature for a 120-nm coating thickness of Eudragit® polymer (a) pull-off force measured with the SFA using a maximum compression force of 1 mN, a measurement speed of 0.75 μm/min and a contact time of 1 min, and (b) comparison of the estimated maximum force obtained for different polymer thicknesses and temperatures with other types of forces.[49]

The van der Waals force was calculated using with $A_H = 6.5 \times 10^{-20}$ J, while the capillary force was calculated using a surface tension of $\gamma = 72.8 \times 10^{-3}$ N.m^{-1} and perfect wetting. The weight is for a particle density of 1.5×10^3 kg.m^{-3}. [Color figure can be viewed in the online issue, which is available at wileyonlinelibrary.com.]

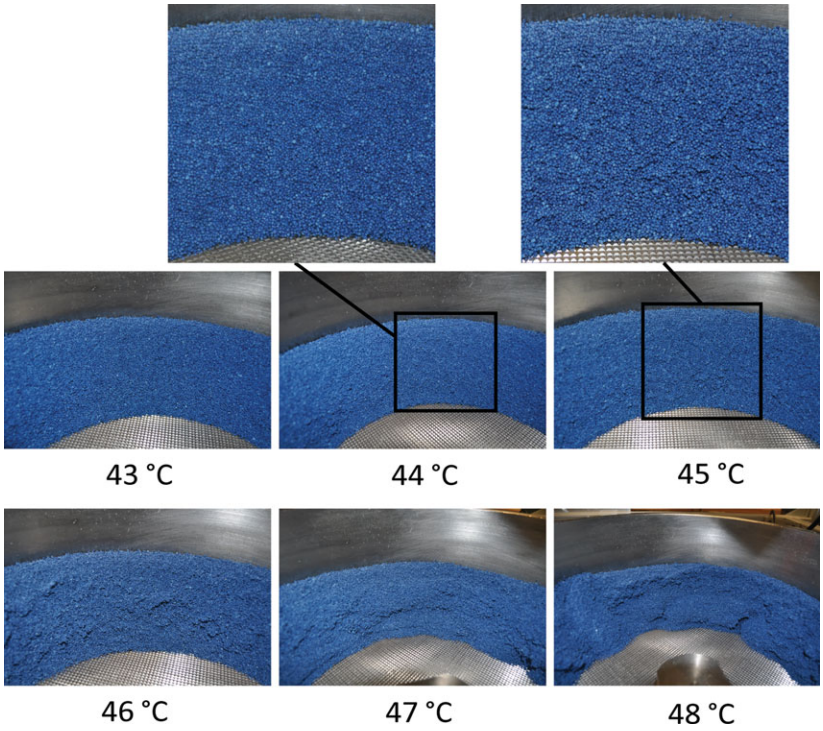

Figure 11. Evolution of the thinly coated particles with respect to the temperature.

The figure insets corresponding to 44 and 45°C show the presence of agglomerates at the surface of the torus. [Color figure can be viewed in the online issue, which is available at wileyonlinelibrary.com.]

breaking phenomenon described. When the temperature continued to rise toward 44°C, the secondary layer consolidated itself. The generation of agglomerates from the detachment of fragments of this layer also ceased. At this point, the flow of particles occurred in an apparent periodic fashion characterized by the growth of the secondary layer until it reached the spheronizer disk where it collapsed and merged with the vanishing free-flowing layer. Once the secondary layer was

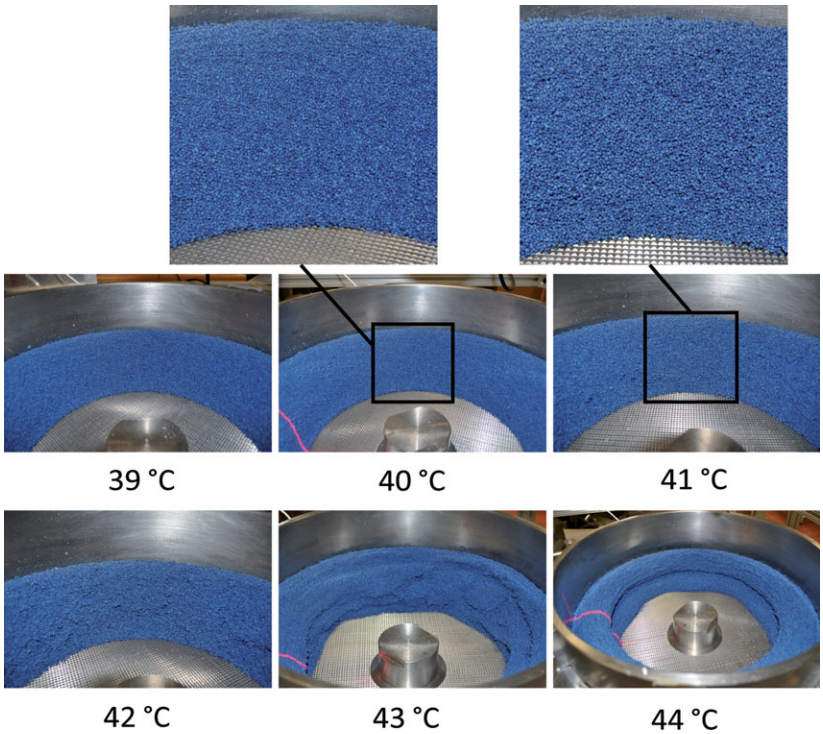

Figure 12. Evolution of the thickly coated particles with respect to the temperature.

The figure insets corresponding to 40 and 41°C show the presence of agglomerates at the surface of the torus. The red beam generated by the laser sheet profiler is apparent at 40, 43 and 44°C. [Color figure can be viewed in the online issue, which is available at wileyonlinelibrary.com.]

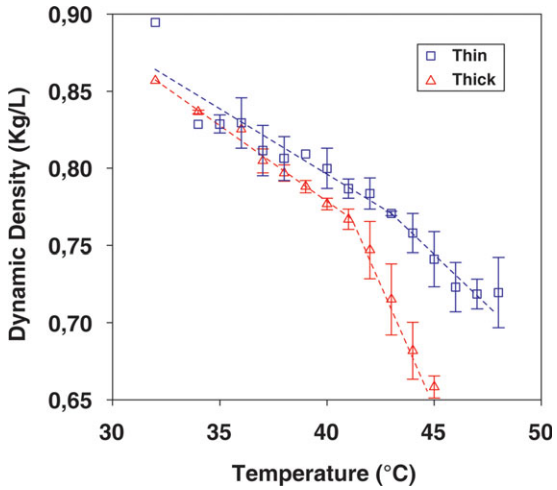

Figure 13. Graph of the particle dynamic density with respect to the temperature for thinly and thickly coated particles.

[Color figure can be viewed in the online issue, which is available at wileyonlinelibrary.com.]

completely broken, it reappeared in the vicinity of the spheronizer wall at the top of the flowing layer, which initiated a new cycle. When the temperature was increased above 44°C, this periodic flow behavior was replaced by a solid-mass motion of the particle bed.

The threshold temperature at which the change in torus morphology occurred appeared to depend on the quantity of polymer coated on the particles. More precisely, the decrease in the coating thickness led to an increase in this threshold temperature, as well as an increase in the temperature range within which the changes of cohesive flow behavior were observed. Contrary to the thickly coated particles, the periodic flow behavior was not observed for the temperature range investigated with the thinly coated particles. The observation of the torus morphologies led to the conclusion that, at a given temperature, a thinner polymer layer results in lower cohesion forces between the particles. Therefore, the appearance of a secondary flow layer for the thin coating would require a temperature that surpasses the range investigated. The results presented here show that cohesive forces generated with the proposed approach can be adjusted with two key parameters that are the temperature and the thickness of the polymer layer. Also, different flow behaviors can be induced depending on the intensity of the cohesive forces during the spheronizer operation.

The flowability of particles can be assessed by different indicators, such as the dilatational effect encountered for a particle bed in motion[50] or by bulk density measurements using the Hausner ratio.[51] A volume dilatation of a particle bed or a reduction of its bulk density is observed when particles at rest enter into a flowing state.[50] When free-flowing material is considered, which means that the interparticle forces are negligible, the volume expansion comes from the collisional forces between the particles as the material moves in a dense flow regime. In the case of cohesive material, for a given shear stress, the dilatation of the particle bed depends on the interparticle forces, which depend themselves on particle properties such as the size, the density, the moisture content and the surface roughness.[51–52]

Figure 13 shows the particle-bed dynamic density measured (mass of the particle bed divided by the volume of the torus calculated from the surface profile) for the thinly and thickly coated particles as a function of the temperature. The dynamic density decreases slowly in a linear fashion with the temperature as long as agglomerates are absent. As the cohesion forces increase causing the agglomeration of particles, the linear decrease in the dynamic density is accentuated by the expansion of the volume of the torus due to the presence of larger particle clusters. It can also be noticed that the mean value of the dynamic density is lowered by the increase in coating thickness. For the thick coating case, the sudden change in the slope of the dynamic density curve is more important because the occurrence of agglomerates was more significant than for the thin coating case. The larger cohesive forces created agglomerates that were more resistant to the spheronizer shear stress. This led to the creation of larger clusters that enhanced the expansion of the torus volume.

Fluidized-bed behavior with coated particles

The most common approach to determine the fluidization state of a system consists of analyzing the bed pressure drop as a function of the superficial gas velocity U_g. The ratio can be used as a first indication of the effect of the interparticle forces on the fluidization behavior.[53] Figure 14 shows, by comparing the pressure-drop curves for the uncoated (SB) and coated (CSB20, CSB30, CSB40) sugar beads, that the overshoot generally observed at U_{mf} (minimum fluidization velocity) is enhanced by the interparticle forces.[54] In particular, for the CSB40 case, it was observed that the relatively strong cohesive forces influenced the bed behavior considerably, with the presence of a large mass of agglomerated particles that got lifted in the column. This phenomenon results in an increase in the pressure drop when U_g is larger than around 0.4 m/s.

Furthermore, a decrease in the pressure drop ratio below unity when a bed is fluidized is known to indicate the degree of cohesiveness in the system.[4,53] As can be seen in Figure 14, the ratios below one are similar for the SB and CSB20 cases, whereas the ratio is significantly smaller than one for

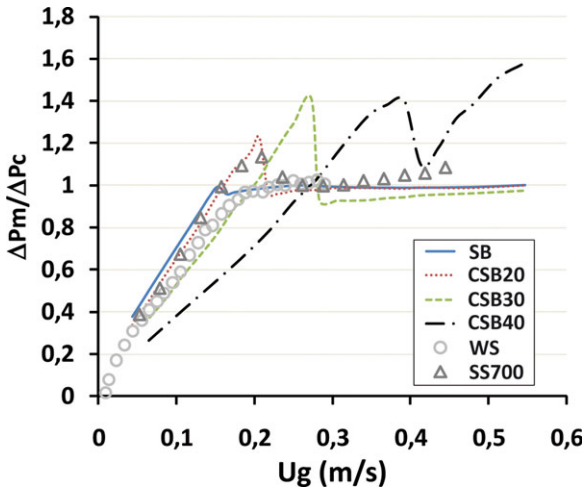

Figure 14. The effect of temperature on a normalized pressure drop profile for the fluidization of coated sugar beads (CSB) at 20, 30 and 40°C and uncoated sugar beads (SB) at 20°C.

Other particles appear in the graph: free-flowing walnut shells (WS)[54] and cohesive silica sand particles (SS) at 700°C[48].

Table 8. Variation of the Fixed-Bed Height for the Uncoated and Coated Sugar Beads

	Fixed bed height (cm)
SB	20.3
CSB20	20.5
CSB30	21.4
CSB40	23.0

the CSB30 case. For the CSB40 case, the ratio remains above one because fluidization is flawed, as explained previously. These results show that the enhancement of cohesive forces can cause the behavior of the particles to change from Group B to Group A and even to Group C. Formisani et al.[12] noted that the voidage of a loosely settled bed of Groups A and B particles increases with increasing temperature. They attributed this phenomenon to the increase in cohesive forces with temperature. Table 8 reports the variation of the fixed-bed height for the uncoated and coated particles. It reveals that the fixed-bed height and, equivalently, the fixed-bed voidage increase with the magnitude of the cohesive forces. This result confirms the findings of Formisani et al.[12] and indicates that the amount of gas that can be held by a fixed bed increases with increasing cohesive forces between particles.

Comparison of the polymer coated particles (CSB20, CSB30, CSB40) with the free flowing (SB and WS) and the cohesive (SS) particles reveals that one can control the flowing behavior by setting an approximate temperature. In particular, one can see in Figure 14 that the CSB20 particles mimic the behavior observed for the silica sand particles heated at 700°C. It indicates that it would be possible to study the effect of interparticle forces on the particle flow behavior encountered in a fluidized bed operated at high temperature by investigating the behavior of coated particles in the same bed but at much small temperature. In this context, the difficulty of assessing such high-temperature processes can be significantly reduced because resorting to a phenomenologically similar low-temperature process makes it possible to use characterization methods based on immersed probes.[56–57]

Conclusion

This work shows that by coating inert particles with a layer of a PEA/PMMA copolymer, the cohesive forces can be modified by a change in the process temperature. The interaction forces between the particles were observed to strengthen with the temperature. This polymer coating approach constitutes a new and different technique to study cohesive particle flow behavior. The introduction of cohesion by heating polymer coated particles can be employed in different types of equipment, such as blenders or fluidized beds. Since it is possible to adjust the magnitude of the cohesive forces with this approach, it can be used to provide valuable information on the flow patterns at various times, in granulators for example, in which particle cohesion changes considerably during the process. A thorough SFA characterization of the force between PEA/PMMA layers with respect to the strain and stress applied as well as the time of contact between these layers was recently achieved and will be published in a near future. This study will allow the effect of contacting time and rate to be determined and will help to implement an appropriate cohesive force model for the discrete element simulation of the particle flow dynamics in the spheronizer as well as in other processes.

Acknowledgments

The financial support of the Natural Science and Engineering Research Council of Canada (NSERC), Merck Frosst of Canada, and Ratiopharm is gratefully acknowledged. We would also like to acknowledge Dr. Eric Charreault for measuring the cohesive forces with the SFA. Finally, we thank Jaber Shabanian for his help with the fluidized bed.

Literature Cited

1. Forsyth AJ, Hutton S, Rhodes MJ. Effect of cohesive interparticle force on the flow characteristics of granular material. *Powder Technol*. 2002;126(2):150–154.
2. Herminghaus S. Dynamics of wet granular matter. *Adv Physics*. 2005;54(3):221–261.
3. Rognon PG, Roux JN, Naaim M, Chevoir F. Dense flows of cohesive granular materials. *J Fluid Mech*. 2008;596:21–47.
4. Geldart D, Harnby N, Wong AC. Fluidization of cohesive powders. *Powder Technol*. 1984;37(1):25–37.
5. Rhodes MJ, Wang XS, Forsyth AJ, Gan KS, Phadtajaphan S. Use of a magnetic fluidized bed in studying Geldart Group B to A transition. *Chem Eng Sci*. 2001;56(18):5429–5436.
6. Seville JPK, Clift R. The effect of thin liquid layers on fluidisation characteristics. *Powder Technol*. 1984;37(1):117–129.
7. Yates JG, Lettieri P, Newton D. The influence of interparticle forces on the fluidization behaviour of some industrial materials at high temperature. *Powder Technol*. 2000;110(1–2):117–127.
8. Lekhal A, Conway SL, Glasser BJ, Khinast JG. Characterization of granular flow of wet solids in a bladed mixer. *AIChE J*. 2006;52(8):2757–2766.
9. Figueroa I, Li HM, Mccarthy J. Predicting the impact of adhesive forces on particle mixing and segregation. *Powder Technol*. 2009;195(3):203–212.
10. Li HM, McCarthy JJ. Phase diagrams for cohesive particle mixing and segregation. *Phys Rev E*. 2005;71(2):021305.
11. Li HM, McCarthy JJ. Cohesive particle mixing and segregation under shear. *Powder Technol*. 2006;164(1):58–64.
12. Formisani B, Girimonte R, Mancuso L. Analysis of the fluidization process of particle beds at high temperature. *Chem Eng Sci*. 1998;53(5):951–961.
13. Hamaker HC. The London-van der Waals attraction between spherical particles. *Physica IV*. 1937;10:1058.
14. Butt H-J, Michael K. *Surface and interfacial forces*. Weinheim: Wiley-VCH Verlag GmbH & Co. KGaA; 2010.
15. Forsyth AJ, Hutton SR, Osborne CF, Rhodes MJ. Effects of interparticle force on the packing of spherical granular material. *Phys Rev Lett*. 2001;87(24):244301.
16. Richefeu V, El Youssoufi MS, Peyroux R, Radjai F. A model of capillary cohesion for numerical simulations of 3D polydisperse granular media. *Int J Numer Anal Met*. 2008;32(11):1365–1383.
17. Soulie F, El Youssoufi MS, Cherblanc F, Saix C. Capillary cohesion and mechanical strength of polydisperse granular materials. *Eur Phys J E*. 2006;21(4):349–357.
18. Iveson SM, Beathe JA, Page NW. The dynamic strength of partially saturated powder compacts: the effect of liquid properties. *Powder Technol*. 2002;127(2):149–161.
19. Weigert T, Ripperger S. Calculation of the liquid bridge volume and bulk saturation from the half-filling angle. *Part Part Syst Char*. 1999;16(5):238–242.
20. Radjai F, Richefeu V. Bond anisotropy and cohesion of wet granular materials. *Philos Trans R Soc Math Phys Eng Sci A*. 2009;367(1909):5123–5138.
21. Lumay G, Vandewalle N. Flow of magnetized grains in a rotating drum. *Phys Rev E*. 2010;82(4):040301.
22. Peters F, Lemaire E. Cohesion induced by a rotating magnetic field in a granular material. *Phys Rev E*. 2004;69(6):061302.
23. Lumay G, Vandewalle N. Controlled flow of smart powders. *Phys Rev E*. 2008;78(6):061302.
24. Packham DE. Surface energy, surface topography and adhesion. *Int J Adhes Adhes*. 2003;23(6):437–448.
25. Dave R, Chen YH, Jallo L, Quintanilla MAS. Characterization of particle and bulk level cohesion reduction of surface modified fine aluminum powders. *Colloid Surface A*. 2010;361(1–3):66–80.

26. von Rohr PR, Spillmann A, Sonnenfeld A. Flowability modification of lactose powder by plasma enhanced chemical vapor deposition. *Plasma Process Polym.* 2007;4:S16–S20.
27. Maeda N, Chen N, Tirrell M, Israelachvili JN. Adhesion and friction mechanisms of polymer-on-polymer surfaces. *Science.* 2002; 297(5580):379–382.
28. Sinha SK, Briscoe BJ. *Polymer Tribology.* London, UK: Imperial College Press; 2009.
29. Fleer GJ. *Polymers at Interfaces.* London, UK: Chapman & Hall; 1998.
30. Dillard DA, Pocius AV. *The Mechanics of Adhesion.* Amsterdam, The Netherlands: Elsevier; 2002.
31. Qiu H, Bousmina M. Determination of mutual diffusion coefficients at nonsymmetric polymer/polymer interfaces from rheometry. *Macromolecules.* 2000;33(17):6588–6594.
32. Chen NH, Maeda N, Tirrell M, Israelachvili J. Adhesion and friction of polymer surfaces: The effect of chain ends. *Macromolecules.* 2005;38(8):3491–3503.
33. Gell CB, Graessley WW, Fetters LJ. Viscoelasticity and self-diffusion in melts of entangled linear polymers. *J Polym Sci Pol Phys.* 1997; 35(12):1933–1942.
34. Kunz K, Stamm M. Initial stages of interdiffusion of PMMA across an Interface. *Macromolecules.* 1996;29(7):2548–2554.
35. Andreozzi L, Castelvetro V, Faetti M, Giordano M, Zulli F. Rheological and thermal properties of narrow distribution poly(ethyl acrylate)s. *Macromolecules.* 2006;39(5):1880–1889.
36. Schach R, Creton C. Adhesion at interfaces between highly entangled polymer melts. *J Rheol.* May-Jun 2008;52(3):749–767.
37. Johnson KL. Contact mechanics. 1985; http://www.knovel.com/knovel2/Toc.jsp?BookID=2685.
38. Barthel E. Adhesive elastic contacts: JKR and more. *J Phys D Appl Phys.* 2008;41(16).
39. Brilliantov NV, Albers N, Spahn F, Poschel T. Collision dynamics of granular particles with adhesion. *Phys Rev E.* 2007;76(5).
40. Liechti KM, Xu DW, Ravi-Chandar K. On the modified Tabor parameter for the JKR-DMT transition in the presence of a liquid meniscus. *J Colloid Interf Sci.* 2007;315(2):772–785.
41. Leger L, Creton C. Adhesion mechanisms at soft polymer interfaces. *Philosophical Trans R Soc Math Phys Eng Sci A.* 2008;366(1869): 1425–1442.
42. Luengo G, Pan J, Heuberger M, Israelachvili JN. Temperature and time effects on the "adhesion dynamics" of poly(butyl methacrylate) (pbma) surfaces. *Langmuir.* 1998;14(14):3873–3881.
43. Silbert LE, Grest GS, Brewster R, Levine AJ. Rheology and contact lifetimes in dense granular flows. *Phys Rev Lett.* 2007;99(6).
44. Timoshenko S, Goodier JN. *Théorie de L'élasticité.* Paris, France: C.Béranger; 1961.
45. Zhang DZ, Rauenzahn RM. Stress relaxation in dense and slow granular flows. *J Rheol.* 2000;44(5):1019–1041.
46. Chau KW, Swei GS. Contact time and interfacial fracture energy of tacky polymers. *J Polym Sci Pol Phys.* 2004;42(16):3013–3025.
47. Heuberger M, Luengo G, Israelachvili J. Topographic information from multiple beam interferometry in the surface forces apparatus. *Langmuir.* 1997;13(14):3839–3848.
48. Wey MY, Lin CL, You SD. The effect of particle size distribution on minimum fluidization velocity at high temperature. *Powder Technol.* 2002;126(3):297–301.
49. Seville JPK, Willett CD, Knight PC. Interparticle forces in fluidisation: a review. *Powder Technol.* 2000;113(3):261–268.
50. Faqih A, Chaudhuri B, Muzzio FJ, Tomassone MS, Alexander A, Hammond S. Flow-induced dilation of cohesive granular materials. *AIChE J.* 2006;52(12):4124–4132.
51. Abdullah EC, Geldart D. The use of bulk density measurements as flowability indicators. *Powder Technol.* 1999;102(2):151–165.
52. Zhu HP, Zhou ZY, Yang RY, Yu AB. Discrete particle simulation of particulate systems: Theoretical developments. *Chem Eng Sci.* 2007;62(13):3378–3396.
53. Lettieri P, Bruni G, Newton D, Barletta D. An investigation of the effect of the interparticle forces on the fluidization behaviour of fine powders linked with rheological studies. *Chem Eng Sci.* 2007;62(1–2):387–396.
54. Shabanian J, Fotovat F, Bouffard J, Chaouki J. Fluidization behavior in a gas-solid fluidized bed with thermally induced inter-particle forces. International Conference on Circulating Fluidized Beds and Fluidization Technology. Sunriver, OR, 2011.
55. Escudero D, Heindel TJ. Bed height and material density effects on fluidized bed hydrodynamics. *Chem Eng Sci.* 2011;66(16):3648–3655.
56. Cui H, Sauriol P, Chaouki J. High temperature fluidized bed reactor: measurements, hydrodynamics and simulation. *Chem Eng Sci.* 2003;58(3–6):1071–1077.
57. Girimonte R, Formisani B. The minimum bubbling velocity of fluidized beds operating at high temperature. *Powder Technol.* 2009; 189(1):74–81.

Manuscript received Nov. 10, 2011, and final revision received Jan. 15, 2012.